Proceedings World Geothermal Congress 2026
Calgary, Canada, June 8 – 11, 2026

Permeability-resistivity relationship across the scale: from lab to the field

Kazuki Sawayama[1]* and Manami Kitamura[2]
Institute for Geothermal Sciences, Kyoto University[1]*, Geological Survey of Japan, National Institute of Advanced Industrial Science and Technology[2]
*E-mail address: sawayama@bep.vgs.kyoto-u.ac.jp

Keywords: Permeability, Electrical resistivity, Rock physics, Fractured reservoir, Enhanced Geothermal System

ABSTRACT

Accurately estimating reservoir permeability is essential for the sustainable development of geothermal resources, including enhanced geothermal systems (EGSs). Recent advances in geophysical techniques have revealed changes in electrical resistivity during EGS development. These changes may be related to spatial and temporal variations in subsurface fluid flow. However, geophysical monitoring data cannot be quantitatively interpreted due to the lack of rock physics models for geothermal reservoirs. Previous studies have shown that changes in permeability can be related to changes in the resistivity of fractured crystalline rocks. Nevertheless, the proposed permeability-resistivity relationships have not been verified using field-scale data from geothermal reservoirs. Therefore, this study aims to investigate the relationship between permeability and resistivity in geothermal reservoir rocks at multiple scales, from the laboratory to field scales. We selected several geothermal areas in Japan as test sites where previous projects obtained field-scale permeability and resistivity data and collected core samples. We conducted the permeability and resistivity measurements under elevated normal stress in the laboratory. Using the measured fracture surface profile, we also generate upscaled fractures and perform numerical simulations to visualize fluid flow and electric current. Consequently, we observed a remarkable inflection in the permeability-resistivity relationship in logarithmic coordinates in each scale. Given that this inflection is related to changes in fracture flow behavior (i.e., percolation), permeability-resistivity relationships might be controlled by the characteristic fracture scale on each scale.

1 INTRODUCTION

In geothermal development, reservoir permeability is a critical indicator for predicting productivity. Typically, high-enthalpy geothermal systems are composed of fracture networks within impermeable host rocks, such as volcanic, hard pyroclastic, and plutonic rocks. These fractures significantly influence the overall flow of the system due to their higher permeability compared to the surrounding host rocks (Kranz et al., 1979; Brace, 1980). Research by Durham (1997) demonstrated that a core sample containing a fracture exhibited permeability 4–7 orders of magnitude greater than that of the host rock at a confining pressure equivalent to a depth of ~3,800 m. This indicates that fractures serve as the main channels for hydrothermal fluid movement, even at potential reservoir depths. Consequently, it is crucial to thoroughly understand fluid flow within rock fractures to ensure the sustainable development of geothermal resources. Additionally, there is an urgent need to develop a technique for monitoring subsurface flow in enhanced geothermal systems (EGSs) to minimize environmental impacts, such as induced seismicity, and to improve recovery efficiency.

Determining the actual permeability of reservoirs during field development is both difficult and expensive. Consequently, many studies have focused on experimentally and numerically characterizing fracture permeability using a single fracture. Traditionally, fractures have been modeled as parallel plates, with the flow's dependence on the distance between these plates (the aperture) described by the cubic law. Witherspoon et al. (1980) investigated the cubic law's validity and concluded that fracture permeability can be uniquely determined by the fracture aperture. However, in rough fractures, flow rates cannot be accurately described using just a single aperture value (Raven and Gale, 1985; Pyrak-Nolte et al., 1988; Glover et al., 1998). Natural fracture surfaces are not smooth parallel plates but are rough and make contact at specific points (Brown and Scholz, 1985; Brown, 1995). These characteristics influence the preferential flow channels within a fracture due to the complexity of the fracture flow system (Watanabe et al., 2008; Ishibashi et al., 2015). Research has consistently shown that fracture permeability is influenced by the microstructural features of fracture surfaces, such as roughness (Zimmerman et al., 1991; Walsh, 1981), contact area (Zimmerman et al., 1992), and tortuosity (Brown, 1989). However, these features cannot be examined under in situ subsurface conditions. Therefore, it is beneficial to develop an alternative method to describe permeability without needing to examining fracture microstructures.

To probe the hydrothermal systems and gain insights into in-situ fluid flow behavior, geophysical observation techniques have been indispensable. For example, the structure of electrical resistivity can indicate the presence of fluids and help estimate subsurface permeability in geothermal and hydrothermal regions (Yamaya et al., 2022; Matsunaga and Kanda, 2022). Monitoring over time has identified variations in seismic velocity and electrical resistivity during geothermal development (Taira et al., 2018; Tsuji et al., 2022; Gunasekera et al., 2003) and during EGS developments (Peacock et al., 2012, 2013; Didana et al., 2017; Johnson et al., 2021, 2024; Feng et al., 2024). These geophysical characteristics alter due to pressure changes, which simultaneously affect fracture apertures and the related subsurface fluid flow system. Since fluid flow and electrical current are described by the diffusion equation (i.e., Darcy's and Ohm's laws), hydraulic and electrical properties are expected to exhibit similar sensitivity to pore microstructures. Although electrical methods are effective for detecting fluid flow in fractures, research on electrical resistivity within fractures is limited, with resistivity-based permeability models primarily developed for porous media (Katz and Thompson, 1986; Glover et al., 2006; Ghanbarian and Male, 2021). In fractured rocks, fluids tend to flow through the critical neck of the aperture (Pyrak-Nolte et al., 1988; Nolte et al., 1989), suggesting that models assuming uniform fluid flow in porous media may not accurately represent fractured geothermal reservoirs. Some field studies have observed unusual changes in the permeability and resistivity of fractured rocks (Park, 1991; Xue et al., 2013), which cannot be accounted for by experimental results from intact rocks, highlighting the significant influence of macroscopic fractures on field-scale phenomena.

Research on the geophysical characteristics of fractured rock masses is limited. Stesky (1986) found a linear relationship between the experimental permeability and conductivity (the inverse of resistivity) in the logarithmic coordinates by using saw-cut fractures as stress increases. Synthetic studies were more conducted due to challenges in achieving repeatability and complete insulation in flow-through tests with rough-walled fractures when measuring resistivity. These studies, which focused on the monotonic reduction of aperture in rough-walled fractures, identified a bilinear relationship (Kirkby et al., 2016; Sawayama et al., 2021a). The differences in these studies stem from the heterogeneous reduction of flow paths caused by surface roughness, which affects the sensitivity of hydraulic and electrical flow to aperture changes (Sawayama et al., 2023). To illustrate this in a laboratory setting, Sawayama and So (2025) developed a method to simultaneously measure the permeability and resistivity of rough-walled fractures, replicating the bilinear relationship. Some field studies have observed that permeability and resistivity respond differently to stress (Pratt et al., 1977), indicating that the slope in permeability–resistivity plots can vary, likely due to the distinct stress sensitivities of each property. Although these findings could connect permeability and resistivity in rough-walled single fractures, a challenge persists: the applicability to real geothermal reservoirs remains uncertain. Currently, no studies have explored the hydraulic-electrical properties of fractured rock masses across different scales, significantly limiting the interpretation of permeability based on electrical observations.

This study aims to explore the multi-scale applicability of the relationship between permeability and electrical resistivity, based on laboratory experiments, borehole logging data, and numerical simulations (intermediate scale).

2 METHOD

2.1 Laboratory experiment

We simultaneously measured the fluid flow, electrical resistivity, and P-wave and S-wave velocities under stress. During the tests, samples were subjected to an effective stress of up to 50 MPa. This covered the stress condition of typical geothermal reservoirs and EGSs (at a depth of ~5 km assuming hydrostatic stress and ~2 km assuming lithostatic stress in granite lithology). In flow-through test, the inlet and outlet pore pressure were controlled using the ISCO syringe pumps. As pore fluid was pumped into the fracture of a jacketed rock sample at constant pressure gradient ∇P, the flow rate Q of the fluid discharged through the fracture was measured. Then bulk permeability k in each stress state was calculated using the Darcy's law as follows:

$$\frac{Q}{A} = -\frac{k}{\mu} \nabla P, \tag{1}$$

where A and μ denote the cross-sectional area and viscosity, respectively.

Resistivity was measured using the electrical impedance method via a four-terminal experimental setup. The current and voltage electrodes were constructed from a silver net ribbon with an AgCl-baked coating (Sawayama and So, 2025). The conductivity of the fluid medium (0.1 mol/L KCl solution) sufficiently surpassed the surface conduction effects within the rock matrix. Electrical impedance Z was given by

$$Z = |Z|e^{i\theta} = Z' + iZ'' = |Z|\cos\theta + i|Z|\sin\theta, \quad (2)$$

where Z' and Z'' denote in-phase (real) and quadrature (imaginary) impedance, respectively, and θ is the phase angle. In this study, the impedance magnitude $|Z|$ and phase angle θ were estimated across a wide frequency spectrum (10^{-1}–10^{5} Hz) on an LCR meter (NF, ZM2376). In general, the electrical impedance of rocks contains resistive and capacitive components. In a simple *RC* parallel circuit, where *R* is resistance and *C* is capacitance, complex impedance Z in the angular frequency ω domain is determined as

$$Z(\omega) = \frac{R}{1 + (RC\omega)^2} - i\frac{R^2C\omega}{1 + (RC\omega)^2}. \quad (3)$$

Combining Eqs. (2) and (3), we obtained

$$\left(Z' - \frac{R}{2}\right)^2 + (Z'')^2 = \left(\frac{R}{2}\right)^2, \quad (4)$$

demonstrating that a plot of Z' versus Z'' on a complex plane forms a semicircular arc (i.e., Cole–Cole circle) that starts from the zero point and centers approximately on the real axis. Based on the curve fitting of Eq.(4), we obtained resistance *R* and subsequently calculates bulk resistivity ρ as follows:

$$\rho = \frac{A}{L}R \quad (5)$$

where *A*/*L* is surface area-to-length ratio.

Acoustic measurements were conducted via the pulse transmission method. Based on the resonant frequency of the transducers, the frequency and amplitude of the input pulse were set to 1 MHz and 10 Vp–p, respectively, using a function generator (NF, WF1974). To improve the signal-to-noise ratio, the transmitted waveforms were amplified using a preamp (NF, 9913) and stacked more than 2000 times. The first arrival times of the P-wave and S-wave were analyzed from the waveforms recorded by an oscilloscope (Yokogawa, DLM5034) using the Akaike information criterion (AIC), where the global minimum of the AIC function corresponds to the onset time of a signal. The AIC criterion requires an appropriate time window, including the waveform regions of interest (Akamatsu et al., 2023; Sarout et al., 2009).

2.2 Meso-scale simulation

To extend the findings from laboratory-scale studies to predictions at the field scale, it is essential to understand the scaling effect on rock physical properties and their interrelations. To achieve this, we simulated synthetic fractures with isotropic surfaces that reflect the fractal nature of actual rock fracture surfaces and adhere to the scaling law of surface roughness (Matsuki et al., 2006; Sawayama et al., 2021b). We utilized the fractal dimension, roughness, and mismatch length scale identified in the natural rock fracture (Sawayama, 2023). Initially, we created a pair of correlated fractal surfaces by performing an inverse Fourier transform on the Fourier components derived from fractional Brownian motion (Brown, 1995). The Fourier components of the footwall $a_{f,xy}$ are a function of the spatial frequency $f = \sqrt{(x^2 + y^2)/L^2}$ in an arbitrary direction according to

$$a_{f,xy} \propto (x^2 + y^2)^{-\frac{4-D}{2}} \exp(2\pi i R_1) \quad (6)$$

where x and y are the node numbers in the x- and y-direction, respectively, and R_1 is a series of uniform random numbers ($0 < R_1 < 1$). Similarly, the Fourier components of the hanging wall $a_{h,xy}$ are

$$a_{h,xy} \propto (x^2 + y^2)^{-\frac{4-D}{2}} \exp\left(2\pi i(R_1 + \gamma(f)R_2)\right) \quad (7)$$

where $\gamma(f)$ represents the frequency-dependent matedness between the two surfaces, and R_2 is a sequence of uniform random numbers that is independent of R_1. The function $\gamma(f)$ takes a value between 0 and 1 to satisfy

$$2\left(1 - \frac{\sin 2\pi\gamma(f)}{2\pi\gamma(f)}\right) = R(f) \quad (8)$$

where $R(f)$ is the ratio of the power spectral densities of the linear profiles between the initial aperture and the surface height of the fracture surface. We determined the function $\gamma(f)$ by solving Eq. (8) using the Newton–Raphson method, using $R(f)$ calculated from the profiles of the natural rock fracture.

As reconstructing the surface roughness of a fracture from the observed spectra is a stochastic process, we examined stochastic fluctuations in models created by ten different random seeds. After taking the inverse Fourier transform of each Fourier component ($a_{f,xy}$ and $a_{h,xy}$), the surface height is adjusted with an arbitrary proportional constant so that the surface roughness σ satisfies the scaling law

$$\sigma = \sigma_0 \left(\frac{L}{L_0}\right)^{3-D} \tag{9}$$

where σ_0 is the standard deviation of the surface height along a linear profile of length L_0 on a fracture surface and σ is the standard deviation of the surface height of an arbitrary fracture of length scale L. In this study, we used L_0 = 24 mm and σ_0 = 0.64 mm from our results for a natural rock fracture and generated 16 m x 16 m scale fracture. After preparing the digital footwall and hanging wall, we created digital fracture models by numerically pairing the fracture walls with different values of aperture closure.

The fracture closure under normal stress was simulated by boundary element method based on a half-space-based dry contact model (Polonsky and Keer, 1999; Sawayama et al., 2023). The numerical solution for the three-dimensional rough contact problem is derived from a Fourier-based discrete formulation with circular convolution. Contact stress arises from the interaction between the two surfaces, and the corresponding surface deflection is the combined elastic deflections of the two surfaces at the contact point. According to Boussinesq's equation, the surface deflection distribution of the rough-on-rough solution is equivalent to rough-on-flat solution (Johnson et al., 1985). To prevent spurious stress concentration along the grid edges, it is assumed that the surface slope is negligibly small across the grid area. The iteration scheme utilizes the conjugate-gradient method, where at each iteration step, the gap distribution is calculated and its mean value is adjusted. The sum of the square of the gap is used to determine the new conjugate steps. In this approach to solving contact problems, the contact area is identified during the iteration process relative to the contact pressure. An upper limit on contact pressure is set to estimate plastic yielding at the most stressed asperity microcontacts. Although this is a relatively simple elastic–plastic model, it often yields more realistic results for rough surfaces compared to a purely elastic contact analysis (Polonsky and Keer, 1999). For this study, we used the following mechanical properties for modeling: Young's modulus of 60 GPa, Poisson's ratio of 0.25, and yield stress of 600 MPa. Additionally, a previous study provided a rigorous mathematical proof of the algorithm's convergence. This ensures that the summation error remains below the discretization error for any number of contact points (Polonsky and Keer, 1999).

For fluid flow simulation, this study employed finite volume method based on a modified local cubic law (MLCL; Brush and Thomson, 2003). This method has been demonstrated to adequately approximate the Navier–Stokes solution, where simple LCL assumes fracture surfaces remain flat parallel. Previous results have indicated that fluid flow through fractures with rough surfaces preferentially follows limited pathways (i.e., channeling flow). This suggests that the parallel plate model cannot accurately represent fluid or electrical flow through fractures. Similar to the fluid flow, electrical conduction through fractures was analyzed by same framework (MLCL) based on resistor network (Kirkby et al., 2016). We assumed electrical conductivity of 5.0 S/m for pore fluid.

2.3 Field scale data compile

To compile the field-scale data, multiple sites were selected as the study area where well tests and electrical logging data were obtained during past NEDO promotional surveys (Geological Survey of Japan, 1991). We collected data from several sites in the Kyushu area of Japan. These reservoirs' feed zones are mainly composed of granitic and andesitic rocks, as well as some mafic rocks. In these surveys, transmissivity (the product of permeability and thickness) was measured by an injection test in potential reservoirs. Using publicly available data, we calculated the average permeability by dividing transmissivity by the reported reservoir thickness. Furthermore, we calculated the bulk resistivity using the average value of the short-normal method in the estimated feed zone, based on electrical logging data from identical sites. Then, we divided this value by the fluid (mud) resistivity to evaluate the formation factor. Based on this database, we collected a total of 37 borehole data to explore the permeability-resistivity relationship on a logging scale.

3 RESULTS

3.1 Permeability and resistivity in laboratory scale

We compiled the relationship between permeability and resistivity of the representative samples (Aji granite, Japan and Belfast diabase, South Africa) from the laboratory experiment. Initial matrix porosity of these samples were 1% and 0.6%, respectively (Sawayama and So, 2025). Overall, permeability is a nonlinear function of resistivity when plotted on logarithmic coordinates, indicating the universal nature of the nonlinear behavior

observed in a numerical study using rough-walled fractures (Sawayama et al., 2023). Although a previous experimental study reported a linear relationship between these two parameters, it only involved two saw-cut fracture samples (Stesky, 1986). Our experimental study with rough-walled fractures suggests that the nonlinear behavior observed in a numerical study (Sawayama et al., 2023) can also be seen in the experimental deformation of naturally fractured crystalline rocks. This discrepancy in results may arise from the rough surfaces of fractures, whereas saw-cut fractures can be considered as parallel plates.

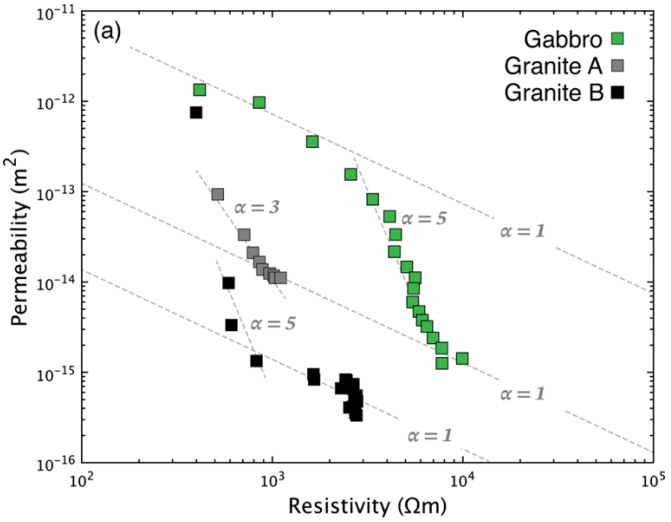


Figure 1. Representative results of log–log correlations between permeability and resistivity in experimental samples. Data from Sawayama and So (2025).

3.2 Permeability and resistivity in meso-scale

The similarity and diversity of changes in permeability and resistivity in different conditions provide the fundamental understanding of the potential linking in these properties. We have then plotted the relationship between permeability and resistivity for upscaled fractures (Fig. 2). At higher permeability levels, the cross-property relationship aligns with the parallel plate model (red line in Fig. 2). Conversely, at lower permeability levels, the relationship diverges from the parallel plate model (star in Fig. 2). These findings indicate that the relationship in meso-scale fractured rock also exhibits inflection.

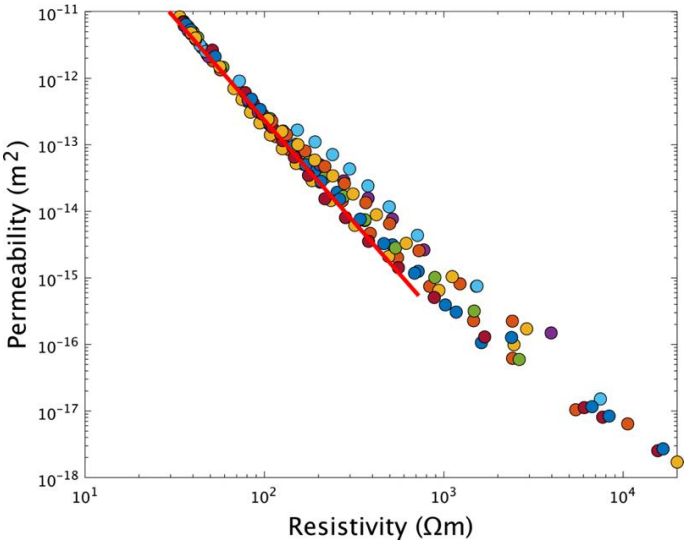


Figure 2 Log–log Relationship between permeability and resistivity in upscaled numerical fractures. Different colors indicate different random seeds. Solid lines indicate values for the parallel plate model.

3.3 Permeability and resistivity in logging-scale

We compiled transmissivity and formation factor retrieved from geothermal development data in several Kyushu area (Oita, Kumamoto, Nagasaki, and Kagoshima prefecture, Japan). Figure 3 shows the relationship between transmissivity and formation factor, demonstrating the inflection in logarithmic relationship. This implies that the slope in permeability-resistivity relationship will be larger in areas with high flow connectivity and smaller in areas with poor flow connectivity, as observed in core scale fracture flow (Sawayama et al., 2023). In other words, differences in resistivity do not directly explain differences in permeability; even when resistivity is slightly higher, reservoir permeability is thought to maintain a relatively high value. While experimental, theoretical, and real data were consistent regarding the inflection behavior, formation factor at the threshold showed different from core scale experiment and meso-scale numerical simulation. Previous study reported that formation factor at the threshold varies with the matrix porosity (Sawayama et al., 2024). Therefore, the discrepancy in the threshold can be attributed to differences in porosity between core scale samples and the reservoir scale.

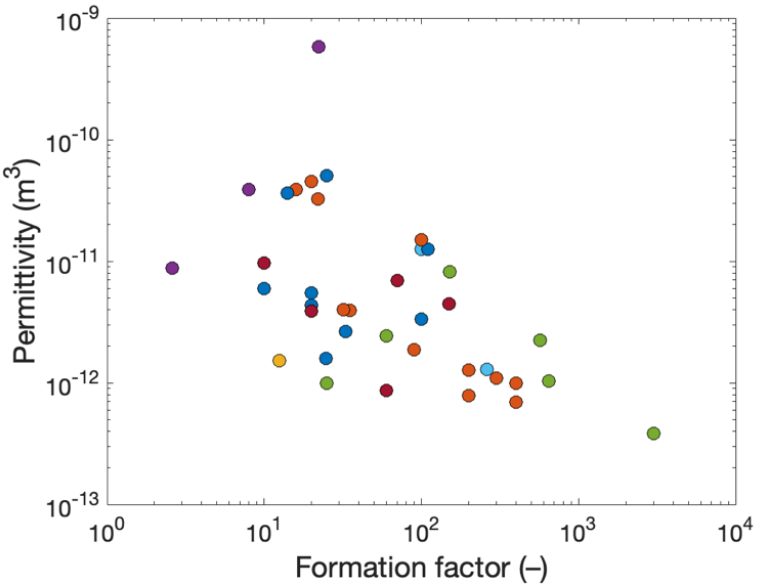


Figure 3 Log–log correlation between transmissivity and resistivity in the wellbore scale in Japanese geothermal development sites (Kyushu area).

4 DISCUSSION

The permeability–resistivity relationships exhibited different trends in each sample. In the equivalent channel model (Walsh and Brace, 1984), this relationship is expressed as a power law as

$$k \propto \rho^{-\alpha} \tag{10}$$

where the slope α is theoretically related to the sensitivity of tortuosity to aperture closure. As α increased, the tortuosity change became more sensitive to the aperture change (Brown, 1989). In granite, α decreased under high stress because tortuosity did not increase after the aperture was sufficiently closed. In contrast, the tortuosity of the gabbro sample continuously increased with increasing aperture closure. Notably, this transition was absent in saw-cut samples (Stesky, 1986), indicating that it originated from the rough surface of the fracture. Although further experimental study is required to clarify the trend in detail, a previous numerical study demonstrated that α does not depend on the fracture surface condition (Sawayama et al., 2023). Through a local flow-path analysis using granite fractures, Sawayama et al. (2023) demonstrated that α changes depend on flow path connection. The value of α becomes unity after dominant flow paths become disconnected, which is consistent with our experimental data under the high-stress condition. Therefore, the nonlinear trend might be related to substantial flow channeling, which is notable in rough-walled fractures. Although future study will elaborate on clarifying this trend with numerous datasets, the important point is that the trend should not be linear when we consider the hydromechanical deformation of naturally fractured crystalline rocks.

5 CONCLUSION

This study investigated the relationship between permeability and electrical resistivity in fractured geothermal reservoir rocks across multiple scales—from laboratory experiments to meso-scale numerical simulations and field-scale logging data analysis. The primary objective was to establish a rock physics basis for quantitatively interpreting geophysical monitoring data in enhanced geothermal systems (EGSs). Our laboratory experiments on rough-walled fractures revealed that permeability and resistivity do not follow a simple linear correlation in logarithmic coordinates, unlike the trends previously reported for saw-cut fractures. Instead, we observed a distinct nonlinear relationship characterized by hysteresis and saturation behavior under high effective stress. This nonlinearity is attributed to the heterogeneous reduction of flow paths caused by fracture surface roughness, which creates preferential flow channeling (percolation) that affects hydraulic and electrical flows differently. These experimental findings were supported by meso-scale numerical simulations, which demonstrated the decoupling of fluid and electrical flow paths. Furthermore, the compilation of field-scale logging data from geothermal fields in Japan exhibited a similar inflection in the transmissivity–formation factor relationship, suggesting that the nonlinear behavior observed in the laboratory is applicable to reservoir-scale fracture networks. Our results indicate that conventional linear models or models derived for porous media are insufficient for characterizing fractured crystalline reservoirs. The inflection behavior in the permeability-resistivity relationship is a critical feature that reflects the connectivity of fracture flow paths. Accounting for this nonlinearity is essential for the accurate estimation of reservoir permeability from electrical resistivity changes detected by geophysical monitoring. These findings provide a crucial step toward establishing more reliable rock physics models for the sustainable development and management of geothermal resources.

Acknowledgements

The present study was supported in part by the Japan Society for the Promotion of Science (JSPS) under JSPS KAKENHI grant numbers JP24K01417 and JP24H01028 and Japan Science and Technology.

REFERENCES

Akamatsu, Y., Nagase, K., Abe, N., Okazaki, K., Hatakeyama, K., Katayama, I.: Cross‐property relationship between electrical resistivity and elastic wave velocity of crustal rocks from the Oman drilling project hole GT3A: Implications for in situ geophysical properties of oceanic crust. J. Geophys. Res. [Solid Earth]. 128, (2023). https://doi.org/10.1029/2022jb026130

Brace, W.F.: Permeability of crystalline and argillaceous rocks. International Journal of Rock Mechanics and Mining Sciences & Geomechanics Abstracts. 17, 241–251 (1980). https://doi.org/10.1016/0148-9062(80)90807-4

Brown, S.R.: Transport of fluid and electric current through a single fracture. J. Geophys. Res. 94, 9429 (1989). https://doi.org/10.1029/jb094ib07p09429

Brown, S.R.: Simple mathematical model of a rough fracture. J. Geophys. Res. 100, 5941–5952 (1995). https://doi.org/10.1029/94jb03262

Brown, S.R., Scholz, C.H.: Broad bandwidth study of the topography of natural rock surfaces. J. Geophys. Res. 90, 12575 (1985). https://doi.org/10.1029/jb090ib14p12575

Brush, D.J., Thomson, N.R.: Fluid flow in synthetic rough-walled fractures: Navier-Stokes, Stokes, and local cubic law simulations. Water Resour. Res. 39, 1085 (2003). https://doi.org/10.1029/2002wr001346

Didana, Y.L., Heinson, G., Thiel, S., Krieger, L.: Magnetotelluric monitoring of permeability enhancement at enhanced geothermal system project. Geothermics. 66, 23–38 (2017). https://doi.org/10.1016/j.geothermics.2016.11.005

Durham, W.B.: Laboratory observations of the hydraulic behavior of a permeable fracture from 3800 m depth in the KTB pilot hole. J. Geophys. Res. [Solid Earth]. 102, 18405–18416 (1997). https://doi.org/10.1029/96JB02813

Durham, W.B., Bonner, B.P.: Self-propping and fluid flow in slightly offset joints at high effective pressures. J. Geophys. Res. 99, 9391–9399 (1994). https://doi.org/10.1029/94jb00242

Feng, Z., Huang, L., Chi, B., Gao, K., Li, J., Ajo-Franklin, J., Blankenship, D.A., Kneafsey, T.J.: Monitoring spatiotemporal evolution of fractures during hydraulic stimulations at the first EGS collab testbed using anisotropic elastic-waveform inversion. Geothermics. 122, 103076 (2024). https://doi.org/10.1016/j.geothermics.2024.103076

Geological Survey of Japan.: Well Data Compiled from Japanese Nation-Wide Geothermal Surveys, Part 2 Logging Data and Geologic Columns Data. Rep.Geol. Surv. Japan. 273 (1991).

Ghanbarian, B., Male, F.: Theoretical power-law relationship between permeability and formation factor. J. Pet. Sci. Eng. 198, 108249 (2021). https://doi.org/10.1016/j.petrol.2020.108249

Glover, P.W., Zadjali, I.I., Frew, K.A.: Permeability prediction from MICP and NMR data using an electrokinetic approach. Geophysics. 71, F49–F60 (2006). https://doi.org/10.1190/1.2216930

Ishibashi, T., Watanabe, N., Hirano, N., Okamoto, A., Tsuchiya, N.: Beyond-laboratory-scale prediction for channeling flows through subsurface rock fractures with heterogeneous aperture distributions revealed by laboratory evaluation. J. Geophys. Res. [Solid Earth]. 120, 106–124 (2015). https://doi.org/10.1002/2014jb011555

Johnson, K.L., Greenwood, J.A., Higginson, J.G.: The contact of elastic regular wavy surfaces. Int. J. Mech. Sci. 27, 383–396 (1985). https://doi.org/10.1016/0020-7403(85)90029-3

Johnson, T.C., Burghardt, J., Strickland, C., Knox, H., Vermeul, V., White, M., Schwering, P., Blankenship, D., Kneafsey, T., the EGS Collab Team: 4D proxy imaging of fracture dilation and stress shadowing using electrical resistivity tomography during high pressure injections into a dense rock formation. J. Geophys. Res. [Solid Earth]. 126, (2021). https://doi.org/10.1029/2021jb022298

Johnson, T.C., Burghardt, J., Strickland, C., Sirota, D., Vermeul, V., Knox, H., Schwering, P., Blankenship, D., Kneafsey, T.: 4D Electrical Resistivity Imaging of Stress Perturbations Induced During High‐Pressure Shear

Kirkby, A., Heinson, G., Krieger, L.: Relating permeability and electrical resistivity in fractures using random resistor network models. J. Geophys. Res. [Solid Earth]. 121, 1546–1564 (2016). https://doi.org/10.1002/2015JB012541

Kranz, R.L., Frankel, A.D., Engelder, T., Scholz, C.H.: The permeability of whole and jointed Barre Granite. International Journal of Rock Mechanics and Mining Sciences & Geomechanics Abstracts. 16, 225–234 (1979). https://doi.org/10.1016/0148-9062(79)91197-5

Matsuki, K., Chida, Y., Sakaguchi, K., Glover, P.W.J.: Size effect on aperture and permeability of a fracture as estimated in large synthetic fractures. Int. J. Rock Mech. Min. Sci. 43, 726–755 (2006). https://doi.org/10.1016/j.ijrmms.2005.12.001

Matsunaga, Y., Kanda, W.: Numerical Modeling of a Volcanic Hydrothermal System Based on Resistivity Structure. Journal of Disaster Research. 17, 654–662 (2022). https://doi.org/10.20965/jdr.2022.p0654

Nolte, D.D., Pyrak-Nolte, L.J., Cook, N.G.W.: The fractal geometry of flow paths in natural fractures in rock and the approach to percolation. Pure Appl. Geophys. 131, 111–138 (1989). https://doi.org/10.1007/BF00874483

Park, S.K.: Monitoring resistivity changes prior to earthquakes in Parkfield, California, with telluric arrays. J. Geophys. Res. [Solid Earth]. 96, 14211–14237 (1991). https://doi.org/10.1029/91JB01228

Peacock, J.R., Thiel, S., Heinson, G.S., Reid, P.: Time-lapse magnetotelluric monitoring of an enhanced geothermal system. Geophysics. 78, B121–B130 (2013). https://doi.org/10.1190/geo2012-0275.1

Peacock, J.R., Thiel, S., Reid, P., Heinson, G.: Magnetotelluric monitoring of a fluid injection: Example from an enhanced geothermal system. Geophys. Res. Lett. 39, 3–7 (2012). https://doi.org/10.1029/2012GL053080

Polonsky, I.A., Keer, L.M.: A numerical method for solving rough contact problems based on the multi-level multi-summation and conjugate gradient techniques. Wear. 231, 206–219 (1999). https://doi.org/10.1016/S0043-1648(99)00113-1

Pratt, H.R., Swolfs, H.S., Brace, W.F., Black, A.D., Handin, J.W.: Elastic and transport properties of an in situ jointed granite. International Journal of Rock Mechanics and Mining Sciences & Geomechanics Abstracts. 14, 35–45 (1977). https://doi.org/10.1016/0148-9062(77)90560-5

Pyrak-Nolte, L.J., Cook, N.G.W., Nolte, D.D.: Fluid percolation through single fractures. Geophys. Res. Lett. 15, 1247–1250 (1988). https://doi.org/10.1029/gl015i011p01247

Raven, K.G., Gale, J.E.: Water flow in a natural rock fracture as a function of stress and sample size. International Journal of Rock Mechanics and Mining Sciences & Geomechanics Abstracts. 22, 251–261 (1985). https://doi.org/10.1016/0148-9062(85)92952-3

Sarout, J., Ferjani, M., Guéguen, Y.: A semi-automatic processing technique for elastic-wave laboratory data. Ultrasonics. 49, 452–458 (2009). https://doi.org/10.1016/j.ultras.2008.12.001

Sawayama, K., So, J.: Electrical resistivity, permeability, and normal stiffness of fractured crystalline rocks: Simultaneous laboratory measurements subjected to hydromechanical loading. Adv. Geo-energy Res. 16, 36–49 (2025). https://doi.org/10.46690/ager.2025.04.05

Sawayama, K., Ishibashi, T., Jiang, F., Tsuji, T.: Relationship between permeability and resistivity of sheared rock fractures: The role of tortuosity and flow path percolation. Geophys. Res. Lett. 50, (2023). https://doi.org/10.1029/2023gl104418

Sawayama, K., Ishibashi, T., Jiang, F., Tsuji, T.: Hydro-mechanical-electrical simulations of synthetic faults in two orthogonal directions with shear-induced anisotropy. J. Rock Mech. Geotech. Eng. 16, 4428–4439 (2024)(a). https://doi.org/10.1016/j.jrmge.2024.08.023

Sawayama, K., Ishibashi, T., Jiang, F., Tsuji, T., Fujimitsu, Y.: Relating Hydraulic–Electrical–Elastic Properties of Natural Rock Fractures at Elevated Stress and Associated Transient Changes of Fracture Flow. Rock Mech. Rock Eng. 54, 2145–2164 (2021a). https://doi.org/10.1007/s00603-021-02391-5

Sawayama, K., Ishibashi, T., Jiang, F., Tsuji, T., Nishizawa, O., Fujimitsu, Y.: Scale-independent relationship between permeability and resistivity in mated fractures with natural rough surfaces. Geothermics. 94, 102065 (2021b). https://doi.org/10.1016/j.geothermics.2021.102065

Stesky, R.M.: Electrical conductivity of brine‐saturated fractured rock. Geophysics. 51, 1585–1593 (1986). https://doi.org/10.1190/1.1442209

Taira, T., Nayak, A., Brenguier, F., Manga, M.: Monitoring reservoir response to earthquakes and fluid extraction, Salton Sea geothermal field, California. Sci Adv. 4, e1701536 (2018). https://doi.org/10.1126/sciadv.1701536

Tsuji, T., Ikeda, T., Matsuura, R., Mukumoto, K., Hutapea, F.L., Kimura, T., Yamaoka, K., Shinohara, M.: Continuous monitoring system for safe managements of CO2 storage and geothermal reservoirs. Sci. Rep. 11, 19120 (2021). https://doi.org/10.1038/s41598-021-97881-5

Walsh, J.B.: Effect of pore pressure and confining pressure on fracture permeability. International Journal of Rock Mechanics and Mining Sciences & Geomechanics Abstracts. 18, 429–435 (1981). https://doi.org/10.1016/0148-9062(81)90006-1

Walsh, J.B., Brace, W.F.: The effect of pressure on porosity and the transport properties of rock. J. Geophys. Res. 89, 9425 (1984). https://doi.org/10.1029/jb089ib11p09425

Watanabe, N., Hirano, N., Tsuchiya, N.: Determination of aperture structure and fluid flow in a rock fracture by high-resolution numerical modeling on the basis of a flow-through experiment under confining pressure. Water Resour. Res. 44, 1–11 (2008). https://doi.org/10.1029/2006wr005411

Witherspoon, P.A., Wang, J.S.Y., Iwai, K., Gale, J.E.: Validity of Cubic Law for fluid flow in a deformable rock fracture. Water Resour. Res. 16, 1016–1024 (1980). https://doi.org/10.1029/wr016i006p01016

Xue, L., Li, H.-B., Brodsky, E.E., Xu, Z.-Q., Kano, Y., Wang, H., Mori, J.J., Si, J.-L., Pei, J.-L., Zhang, W., Yang, G., Sun, Z.-M., Huang, Y.: Continuous permeability measurements record healing inside the Wenchuan earthquake fault zone. Science. 340, 1555–1559 (2013). https://doi.org/10.1126/science.1237237

Yamaya, Y., Suzuki, Y., Murata, Y., Okamoto, K., Watanabe, N., Asanuma, H., Hase, H., Ogawa, Y., Mogi, T., Ishizu, K., Uchida, T.: 3-D resistivity imaging of the supercritical geothermal system in the Sengan geothermal region, NE Japan. Geothermics. 103, 102412 (2022). https://doi.org/10.1016/j.geothermics.2022.102412

Zimmerman, R.W., Chen, D.-W., Cook, N.G.W.: The effect of contact area on the permeability of fractures. J. Hydrol. 139, 79–96 (1992). https://doi.org/10.1016/0022-1694(92)90196-3

Zimmerman, R.W., Kumar, S., Bodvarsson, G.S.: Lubrication theory analysis of the permeability of rough-walled fractures. International Journal of Rock Mechanics and Mining Sciences & Geomechanics Abstracts. 28, 325–331 (1991). https://doi.org/10.1016/0148-9062(91)90597-F